Supporting Information

Inherited Construction of Porous Zinc Hydroxide Sulfate Layer for Stable Dendrite-Free Zn Anodes

Zhicheng Xiang [a], *Yubing Qiu* [a], *Xingpeng Guo* [c], *Kai Qi* *[, a], *Zheng Long Xu* *[, b], and *Bao Yu Xia* *[, a]

[a] School of Chemistry and Chemical Engineering, Key Laboratory of Material Chemistry for Energy Conversion and Storage (Ministry of Education), Hubei Key Laboratory of Material Chemistry and Service Failure, Hubei Engineering Research Center for Biomaterials and Medical Protective Materials, Huazhong University of Science and Technology (HUST), 1037 Luoyu Road, Wuhan 430074, P. R. China

[b] Research Institute of Advanced Manufacturing, Department of Industrial and Systems Engineering, The Hong Kong Polytechnic University, Hung Hom, Kowloon, Hong Kong SAR, China

[c] School of Chemistry and Chemical Engineering, Guangzhou University, Guangzhou, 510006, P. R. China

* Corresponding Author: qikai@hust.edu.cn (K. Qi); zhenglong.xu@polyu.edu.hk (Z. L. Xu); byxia@hust.edu.cn (B. Y. Xia)

Supplementary Experimental

Preparation of Zn@ZHS electrodes. The commercial Zn foil with the thickness of 0.1 mm was cut into Zn disks with the diameter of 14 mm, which were sonicated in ethanol for 5 min. The washed Zn disks were used as the substrates for the growth of ZIF-8 membranes. During the sample preparation, only one side of the Zn disks was exposed to the reaction solution to ensure the conductivity of another side for the subsequent electrochemical experiments. The solution for ZIF-8 growth was prepared by dissolving 0.648 g of 2-methylimidazole and 0.538 g of zinc chloride in 50 mL methanol. The Zn disks were immersed into the solution in a Teflon lined stainless-steel autoclave, which was heated at 120 °C for 24 h and naturally cooled down to room temperature. In this way, the surfaces of Zn disks were covered with thin ZIF-8 membranes. After being washed and dried in vacuum drying oven, the homogeneous Zn@ZIF-8 specimens were obtained, which were subsequently soaked in 2 M $ZnSO_4$ aqueous solution for different times to prepare the Zn@ZHS with various initial structures. Finally, the Zn@ZHS electrodes were obtained after being ultrasonically washed by ethanol and dried in vacuum drying oven.

Characterizations. Scanning electron microscopy (SEM, SU8010, Japan) and Transmission electron microscope (TEM, Talos F200X) were applied for measurements of morphologies and microscopic structures. Atomic force microscope (AFM, SPM9700) was applied to measure roughness and morphologies. Powder X-ray diffraction (XRD) was performed on a Ultima IV-185(Japan) with Cu Kα radiation between 5° and 80° at 10° min^{-1}. Raman spectra were inspected on a Bruker RFS100/S instrument. X-ray photoelectron spectroscopy (XPS) was determined by a Thermo Scientific with Al Kα radiation. Time-of-flight secondary ion mass spectrometry (TOF-SIMS) was performed on a TOF.SIMS 5-100 instrument (IONTOF GmbH). Fourier Transform Infrared Spectroscopy (FTIR) analyzer (TENSOR-27, Germany) was applied to detect the functional groups.

Electrochemical measurements. The cyclic voltammetry (CV), linear voltammetry (LSV) and electrochemical impedance spectroscopy (EIS) were carried out by a CHI760e electrochemical workstation (Chenhua, Shanghai). The galvanostatic charge/discharge measurements were performed on a CT-4008 cell test equipment (Neware, Shenzhen). The cells were assembled in standard CR2032-type coin cells using MnO_2 cathodes, bare Zn or Zn@ZHS anodes, glass fiber separators (Whatman, GF/D) and 2 M $ZnSO_4$ aqueous electrolytes. The EIS was recorded with a frequency range from 0.1 Hz to 10^5 Hz with an A.C. voltage of 5 mV. The CV was conducted with a low scan rate of 1 mV s^{-1}. The LSV and polarization curves were conducted in electrolytic cell (Ag/AgCl and Pt electrode were reference electrode and counter electrode respectively) with a scan rate of 5 mV s^{-1}. Chronopotentiometry is conducted in symmetric cells with a condition of 0.5 mA cm^{-2} for 1 h. Chronoamperometry is conducted in symmetric cells with an overpotential of -150 mV for 400 s. The asymmetric cells were assembled using Ti foil and the Cut-off voltage was 0.5 V. The symmetric cells were assembled using bare Zn or Zn@ZHS as both the working electrode and the counter/reference electrode. The electronic conductivity was tested by a four-point probe equipment (ST2258C).

The Zn^{2+} transference number was evaluated utilizing bare Zn and Zn@ZHS-3h symmetric cells combined by EIS before and after chronoamperometry (CA) test, and calculated by the following equation:

$$t_{Zn^{2+}} = \frac{I_s(\Delta V - I_0 R_0)}{I_0(\Delta V - I_s R_s)}$$

where I_0 and R_0 are the initial current and resistance, respectively. ΔV is the applied voltage polarization (10 mV), I_s and R_s are the steady state current and resistance, respectively.

The calculation of activation energy (E_a) based on electrochemical impedance spectrum (EIS) analysis at different temperatures. The E_a can be quantitatively calculated by the following Arrhenius equation:

$$\frac{1}{R_{ct}} = A\ exp(\frac{-E_a}{RT})$$

where the R_{ct}, E_a, A, R, and T stand for the charge-transfer resistance, the activation energy, the frequency factor, the ideal gas constant, and the temperature in Kelvin.

The ionic conductivity was calculated by following equation:

$$\sigma = \frac{l}{R_b \times S}$$

where l was the thickness of the ZHS membrane, R_b was the resistance according to EIS, and S was the contact area between ZHS and block electrode. During the ionic conductivity measurement, a drop of aqueous $ZnSO_4$ electrolyte was employed for ZHS and glass fiber membranes to reflect the apparent ionic conductivity under the battery working station.

COMSOL Multiphysics simulation and calculation. The electrochemical deposition process of zinc ion at the electrode interface of zinc metal was simulated by the software of COMSOL Multiphysics 5.4. The models of "Secondary current distribution", "Transport of diluted species" and "Deformable Geometry" were utilized. The "Secondary current distribution" and "Transport of diluted species" were coupled by using concentration dependent kinetic equation. In addition, the "Deformable Geometry" interface was coupled to the "Secondary current distribution" by calculating the amount of deposited materials.

Density functional theoretical (DFT) computations. Spin-polarized density functional theory calculations were performed using the DMol^3. Perdew-Burke-Ernzerhof (PBE) exchange-correlation functional within the generalized gradient approximation (GGA) were used in the calculation. A 4×4 supercell Zn surface with four atomic layers was built. During the optimization process, the bottom two layers of atoms are fixed, and the top two layers of atoms are relaxed. A 2×1 supercell $Zn_4(OH)_6SO_4 \cdot 4H_2O$ surface was built. The vacuum layer is set to 15 Å. The *k*-point grid of Zn and $Zn_4(OH)_6SO_4 \cdot 4H_2O$ surfaces are set to 2×2×1 and 2×4×1, respectively. All electron effects were utilized for the core treatment. The double numeric polarization (DNP) basis (4.4) set with a thermal smearing value of 0.005 Ha was used to describe atomic

orbitals. The convergence tolerance of energy, maximum force and maximum displacement were 1.0×10^{-5} Ha, 2.0×10^{-3} Ha/Å and 2.0×10^{-3} Å, respectively. Meanwhile, the DFT-D method was used to describe van der Waals interaction. The binding energies (E_b) of H_2O on Zn and $Zn_4(OH)_6SO_4\cdot4H_2O$ surfaces were calculated by:

$$E_b = E(\text{sub} + H_2O) - E(\text{sub}) - E(H_2O)$$

where $E(\text{sub} + H_2O)$, $E(\text{sub})$ and $E(H_2O)$ are the energies of the substrate with H_2O, the substrate and H_2O, respectively. The stepwise desolvation energies of $[Zn^{2+}(H_2O)_6]$ and $[Zn^{2+}(H_2O)_5SO_4^{2-}]$ were calculated according to (the rest can be done in the same manner):

$$\Delta E = E\{[Zn^{2+}(H_2O)_5]\} + E(H_2O) - E\{[Zn^{2+}(H_2O)_6]\}$$

$$\Delta E = E\{[Zn^{2+}(H_2O)_4SO_4^{2-}]\} + E(H_2O) - E\{[Zn^{2+}(H_2O)_5SO_4^{2-}]\}$$

Supplementary Figures

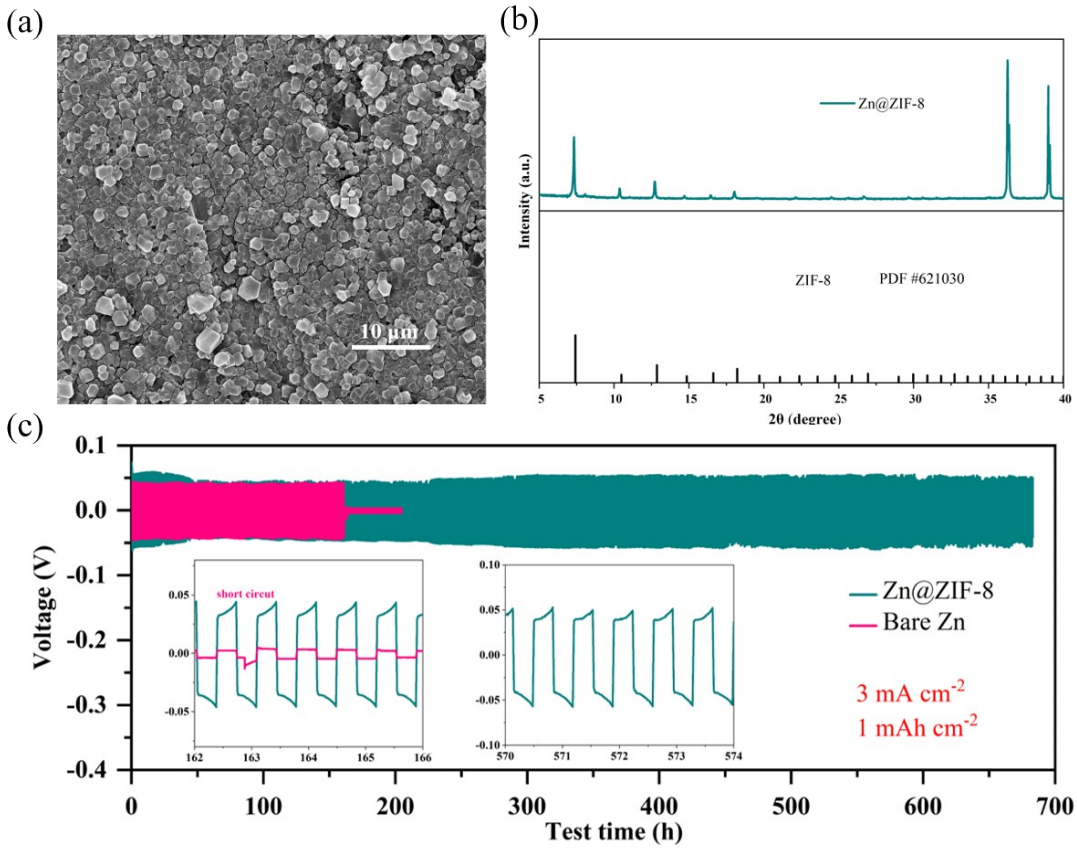

Figure S1. (a) SEM image and (b) XRD pattern of Zn@ZIF-8. (c) Comparison of cycling stability of bare Zn and Zn@ZIF-8 electrodes based symmetric cells in 2 M $ZnSO_4$ electrolytes at 3 mA cm^{-2} with a capacity limitation of 1 mAh cm^{-2}.

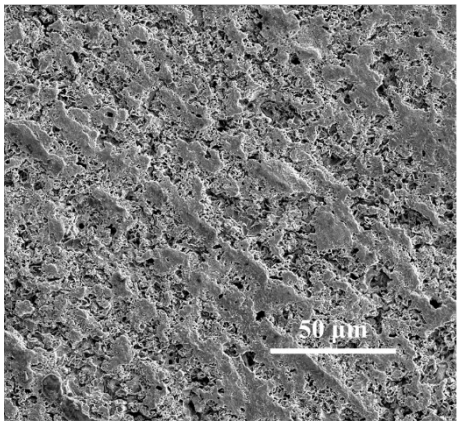

Figure S2. SEM image of Zn@ZIF-8 after cycling in the symmetric cell.

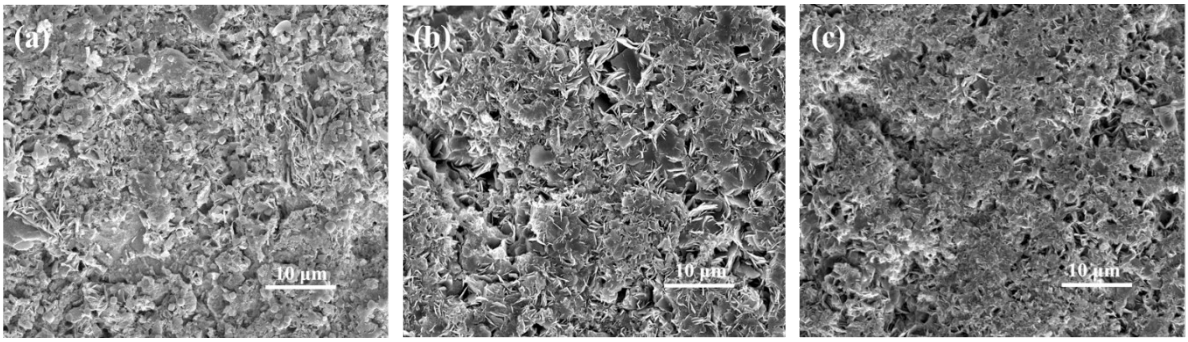

Figure S3. SEM images of Zn@ZIF-8 electrodes standing in freshly-assembled symmetric cells for (a) 5 min, (b) 1 h, and (c) 12 h without the operation of charging/discharging.

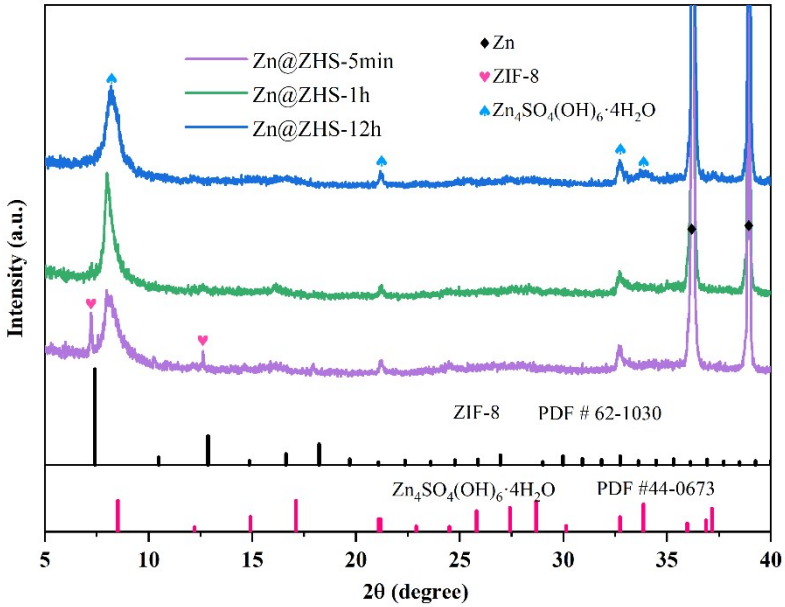

Figure S4. XRD patterns of Zn@ZIF-8 electrodes standing in freshly-assembled symmetric cells for 5 min, 1 h, and 12 h without the operation of charging/discharging.

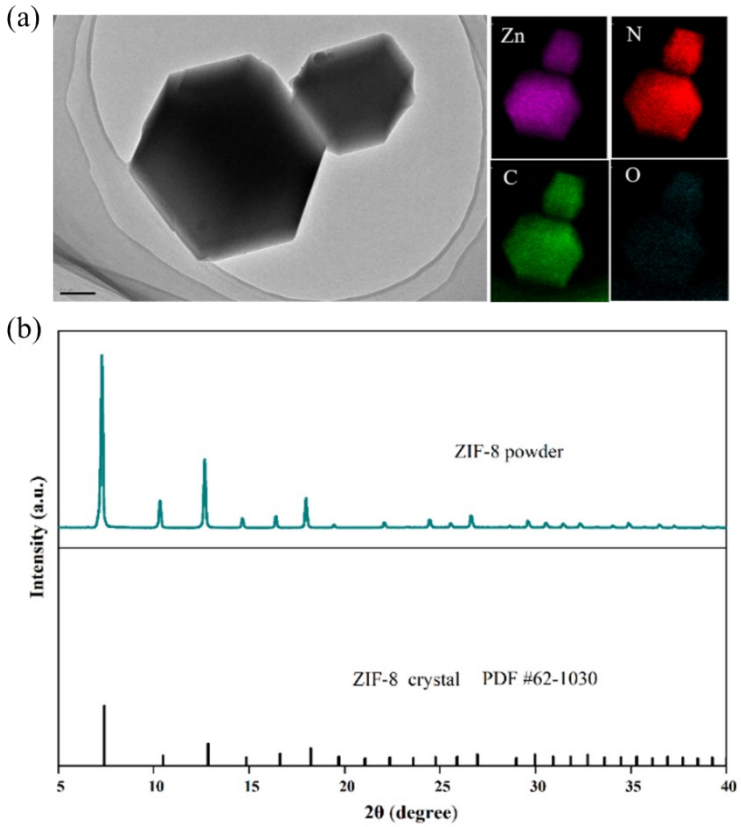

Figure S5. (a) TEM image and elemental mapping and (b) XRD pattern of ZIF-8 powders.

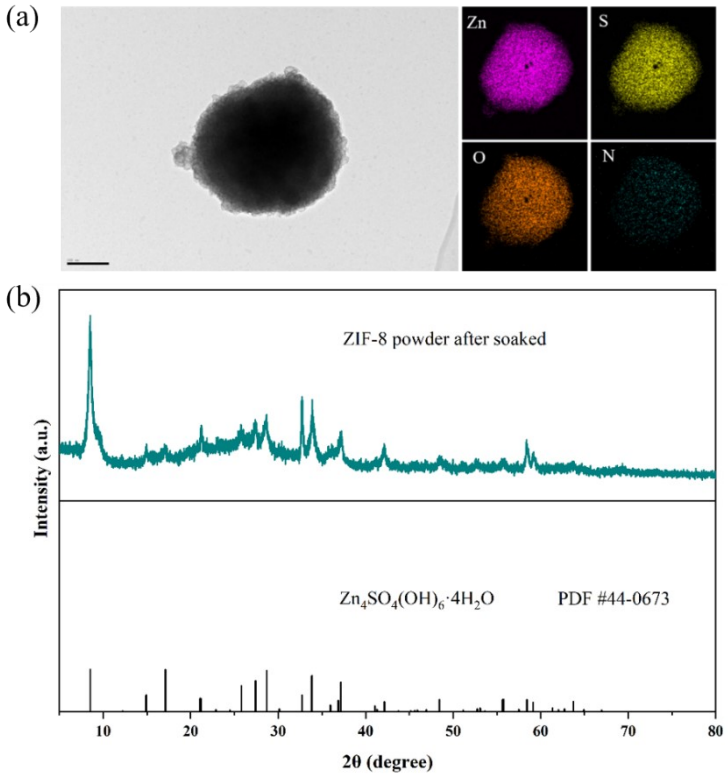

Figure S6. (a) TEM image and elemental mapping and (b) XRD pattern of ZIF-8 powders soaked in 2 M $ZnSO_4$ aqueous solution.

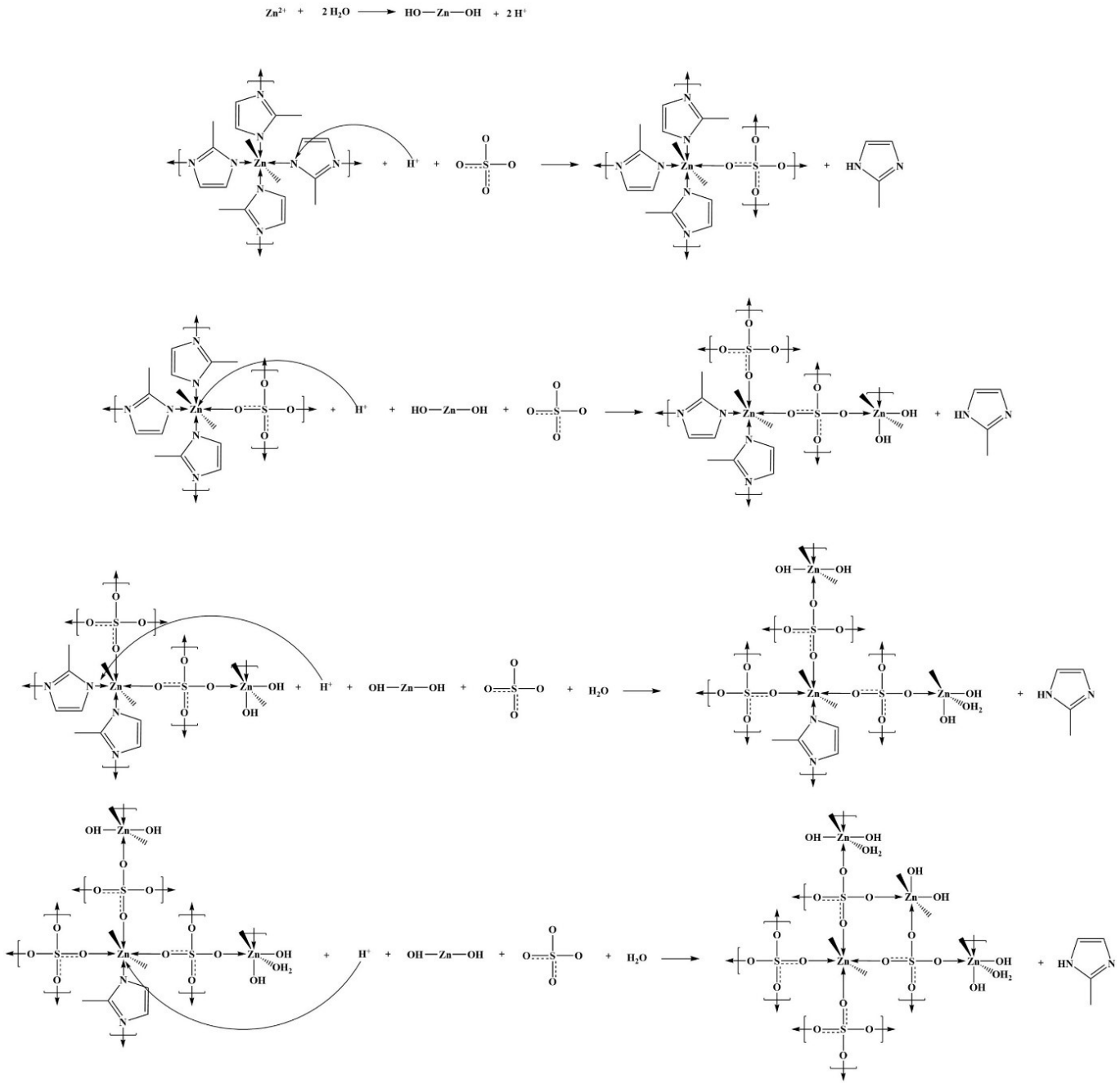

Figure S7. Schematic illustration of the transformation of ZIF-8 to zinc hydroxide sulfate in $ZnSO_4$ electrolyte.

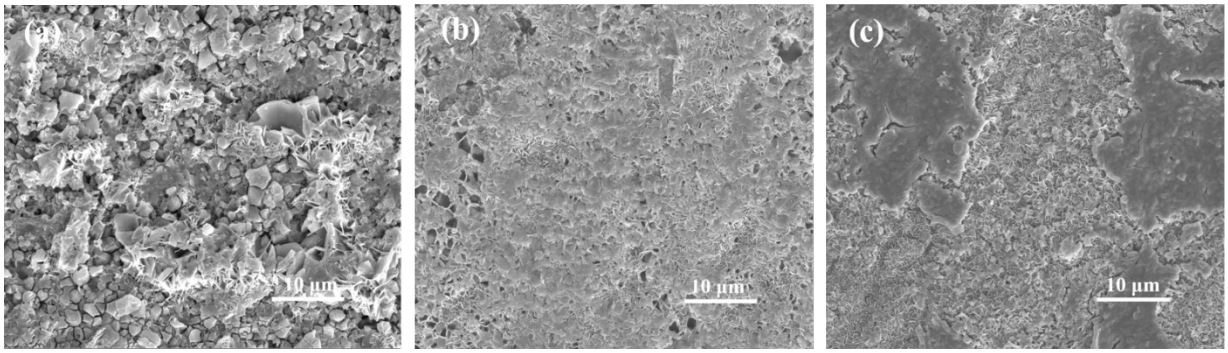

Figure S8. SEM images of (a) Zn@ZHS-15s, (b) Zn@ZHS-12h, and (c) Zn@ZHS-24h.

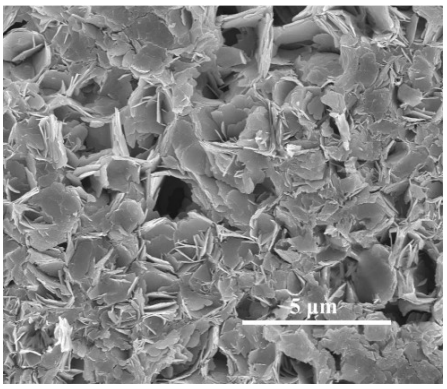

Figure S9. High resolution SEM image of Zn@ZHS-3h.

Figure S10. Contact angles of deionized water on the surfaces of bare Zn, Zn@ZIF-8 and Zn@ZHS-3h.

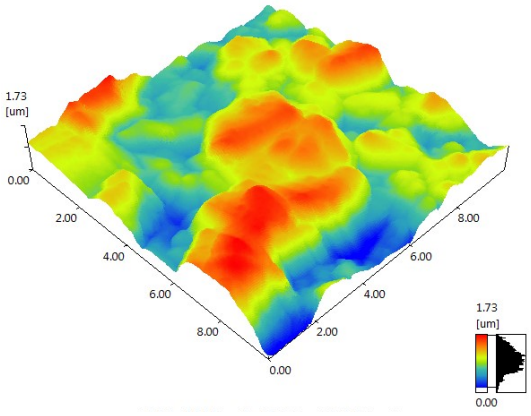

Figure S11. AFM 3D morphology of Zn@ZIF-8.

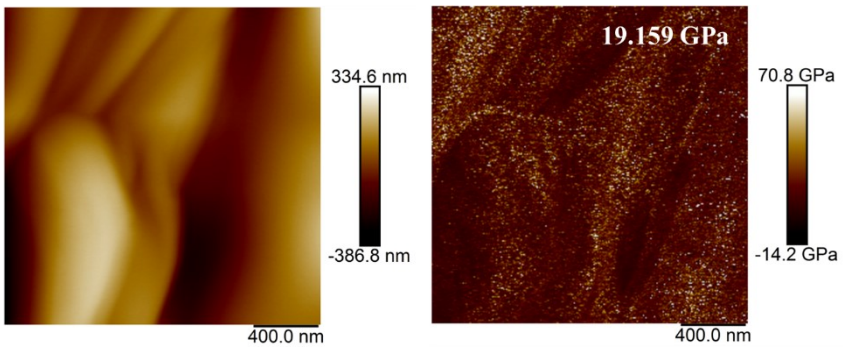

Figure S12. AFM morphology and corresponding Derjaguin-Muller-Toporov (DMT) modulus mapping of Zn@ZHS-3h.

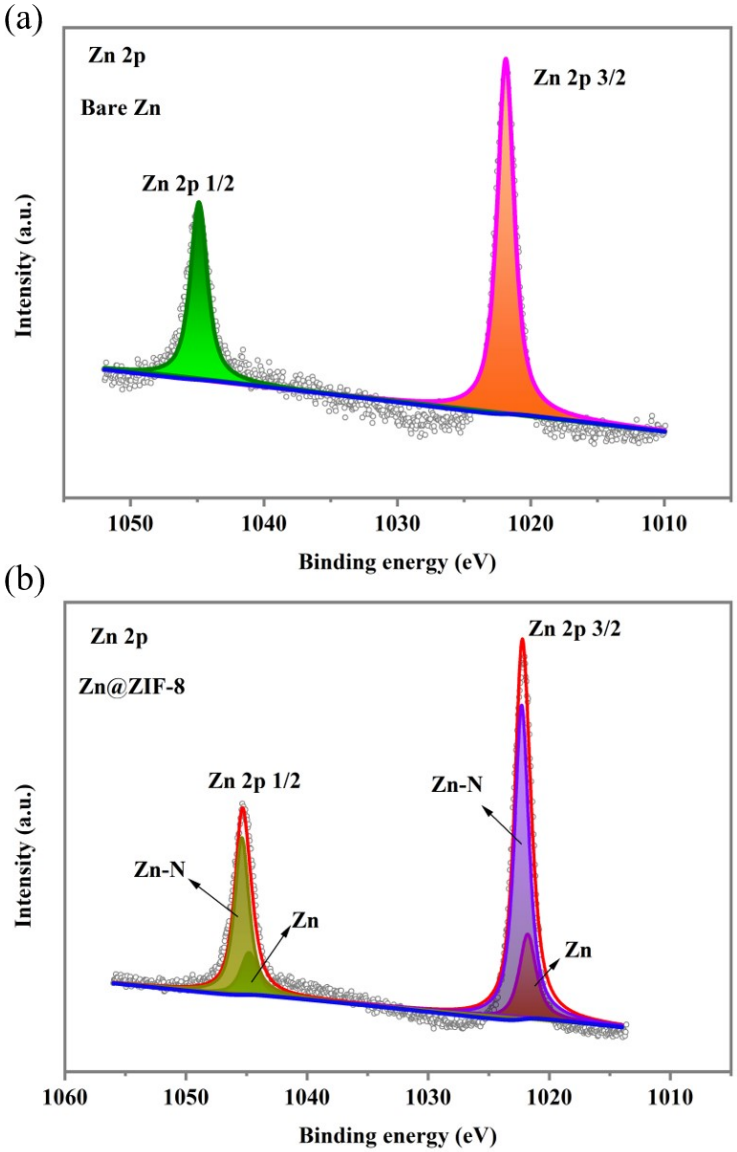

Figure S13. XPS high-resolution Zn 2p spectra of (a) bare Zn and (b) Zn@ZIF-8.

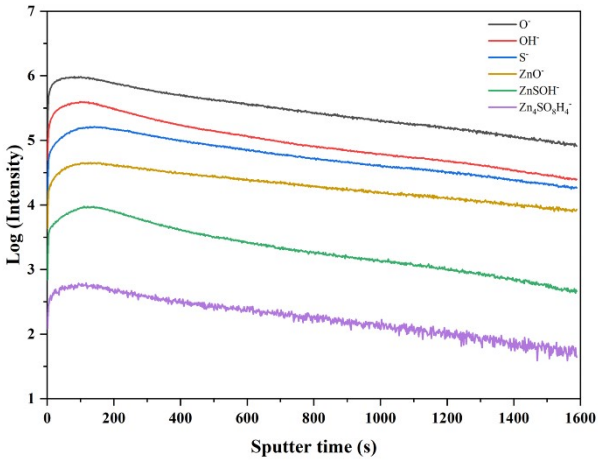

Figure S14. TOF-SIMS depth profiling for the composition of Zn@ZHS-3h.

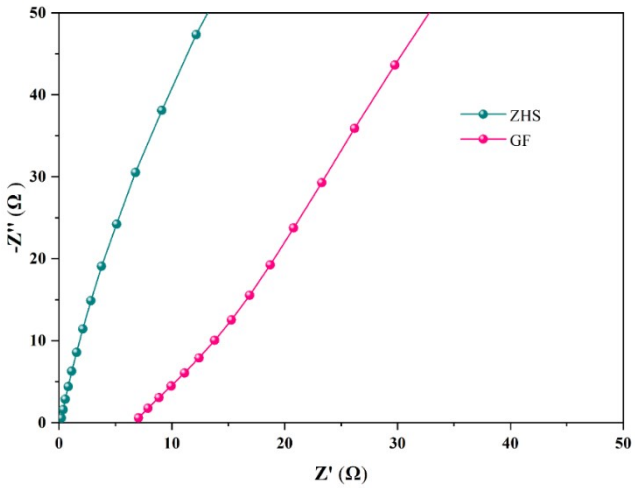

Figure S15. The EIS of glass fiber (GF) separator and ZHS layer based solid electrolytes for the ionic conductivity measurement.

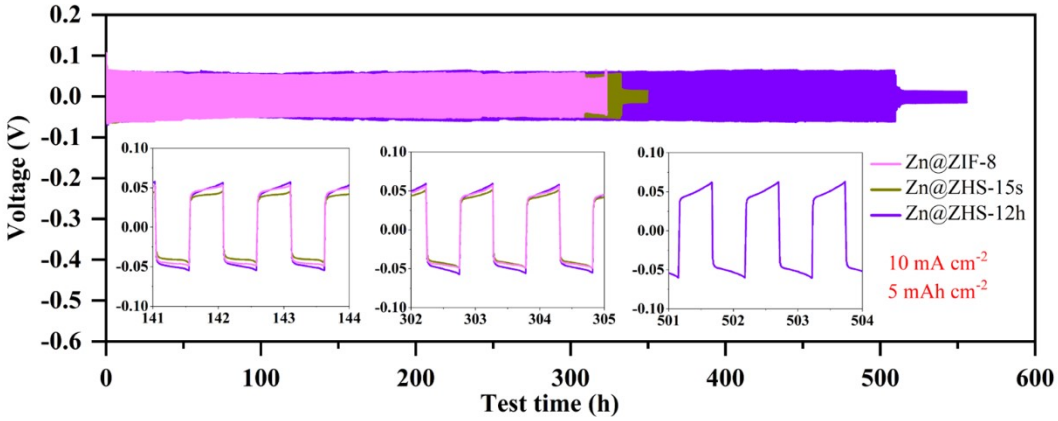

Figure S16. Galvanostatic Zn plating/stripping processes of Zn@ZIF-8//Zn@ZIF-8, Zn@ZHS-15s//Zn@ZHS-15s, Zn@ZHS-12h//Zn@ZHS-12h symmetric cells.

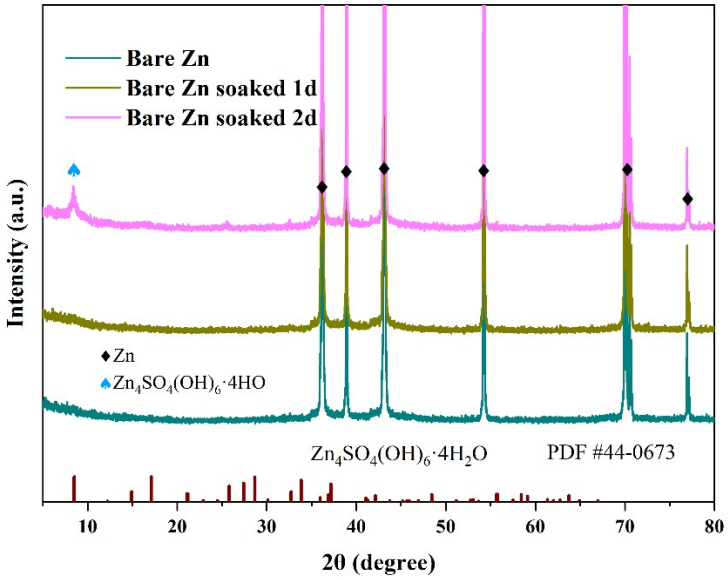

Figure S17. XRD of the bare Zn foils soaked in 2 M $ZnSO_4$ aqueous solution for 1 day and 2 days.

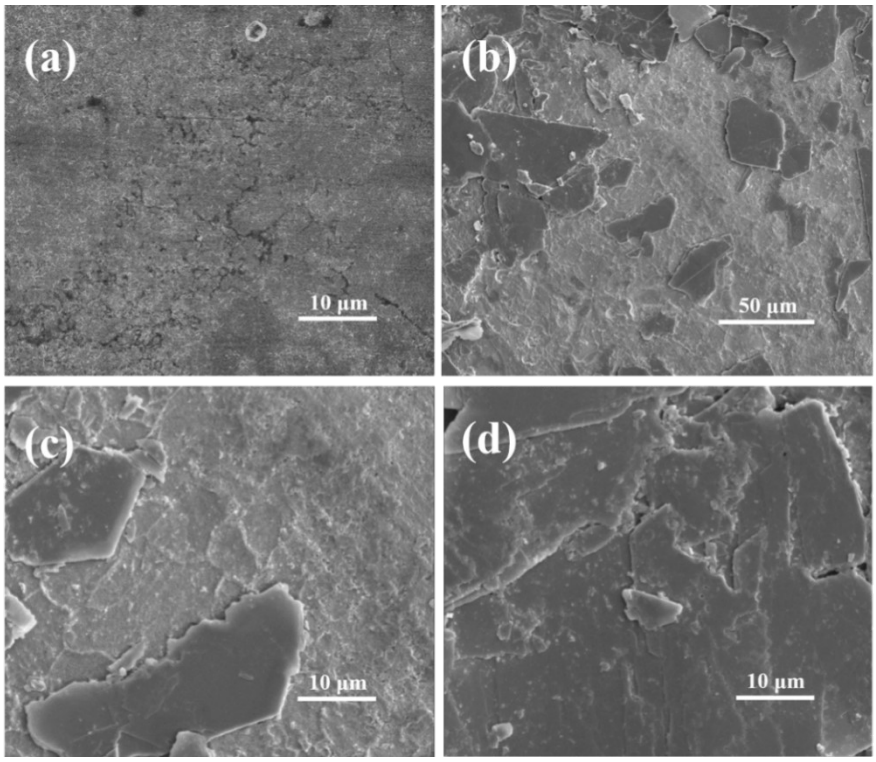

Figure S18. SEM images of (a) bare Zn and (b-d) Zn foils soaked in 2 M $ZnSO_4$ aqueous solution for 2 days.

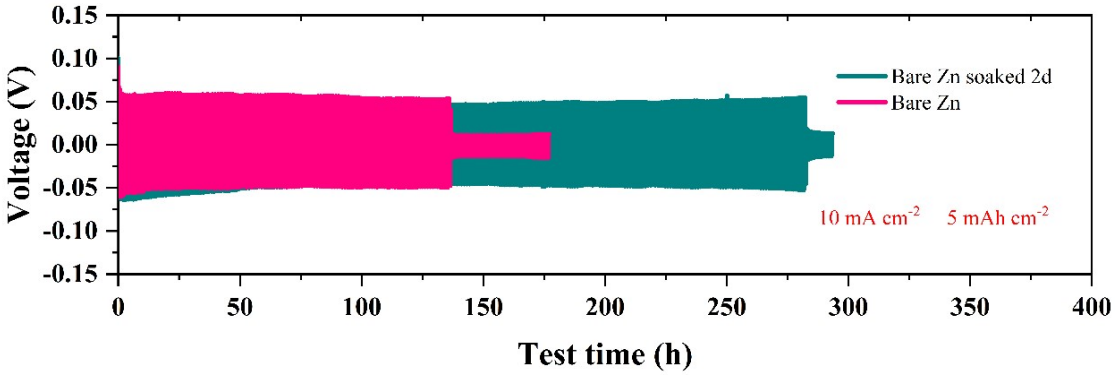

Figure S19. Comparison of cycling stability of bare Zn and corroded Zn symmetric cells at 10 mA cm^{-2} with a capacity limitation of 5 mAh cm^{-2}.

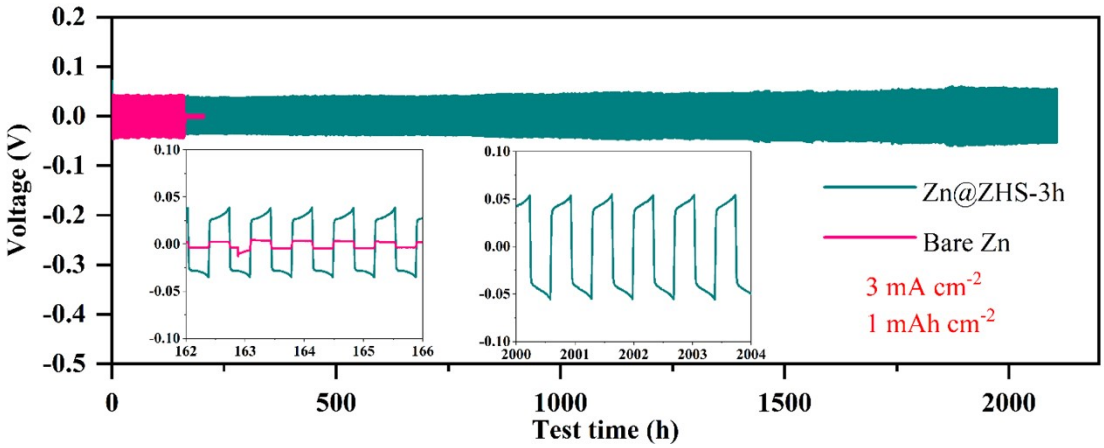

Figure S20. Comparison of cycling stability of bare Zn and Zn@ZHS-3h symmetric cells at 3 mA cm^{-2} with a capacity of 1 mAh cm^{-2}.

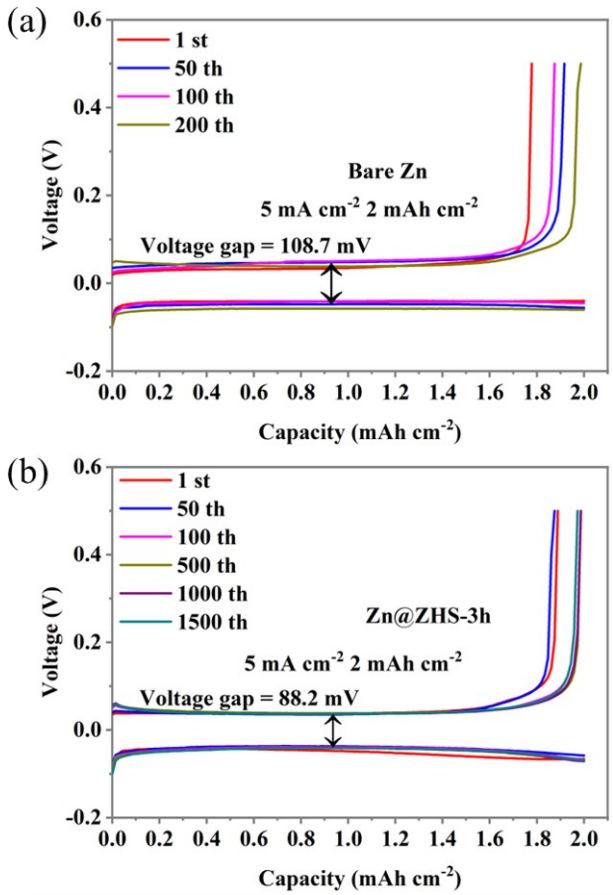

Figure S21. Voltage profiles of the (a) bare Zn//Ti and (b) Zn@ZHS-3h//Ti asymmetric cells cycling at a current density of 5 mA cm^{-1} with a capacity of 2 mAh cm^{-2}.

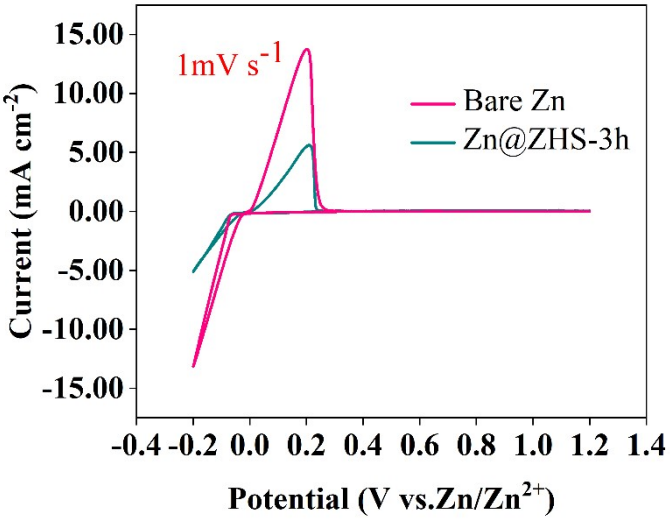

Figure S22. CV curves at a scan rate of 1.0 mV s^{-1} of bare Zn//Ti and Zn@ZHS-3h//Ti cells.

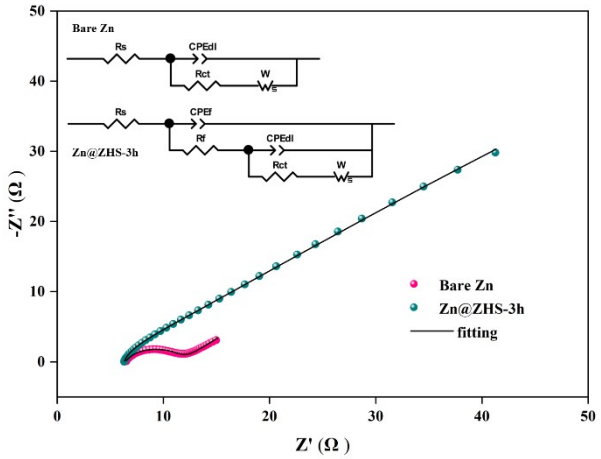

Figure S23. The Nyquist plots of bare Zn and Zn@ZHS-3h electrodes (Ag/AgCl as reference electrode and Pt plate as counter electrode).

The insets are the equivalent circuits (EC) for fitting the Nyquist plots. In the EC for bare Zn electrode, R_s is the solution resistance, CPE_{dl} is the constant phase elements for the electric double layer, R_{ct} is the charge transfer resistance, and W_s is the generalised finite Warburg (GFW) impedance for ion diffusion at the interface. In the EC for Zn@ZHS-3h, CPE_f is the constant phase elements for ZHS layer, R_f is the film resistance of ZHS layer, and other parameters are the same as those in the EC for bare Zn.

Table S1. The fitting parameters of the Nyquist plots in Figure S23.

	R_s	CPE_{dl}	CPE_{dl}	R_{ct}	CPE_f	CPE_f	R_f	W_s
	$\Omega \cdot cm^2$	$mF \cdot cm^{-2}$	/n1	$\Omega \cdot cm^2$	$mF \cdot cm^{-2}$	/n2	$\Omega \cdot cm^2$	$\Omega \cdot cm^2$
bare Zn	6.4	4.2×10^{-4}	0.70	8.8	/	/	/	0.09
Zn@ZHS-3h	11.2	1.8×10^{-4}	0.79	10.2	1.5×10^{-3}	0.89	109.4	0.004

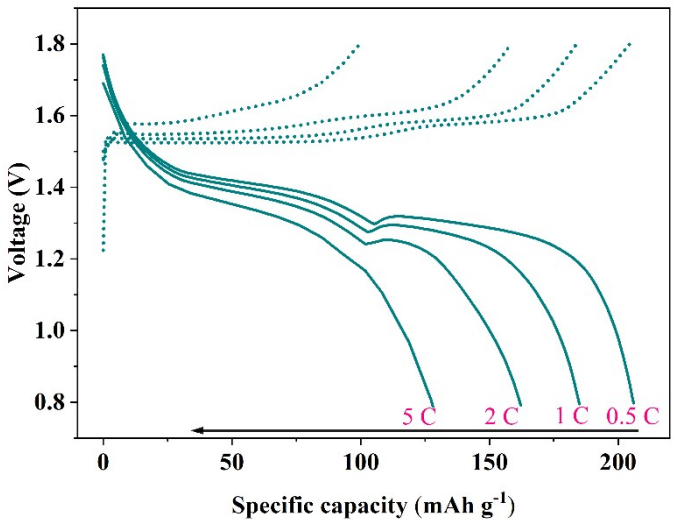

Figure S24. Charge-discharge curves of Zn@ZHS-3h//MnO_2 cell at different current densities.

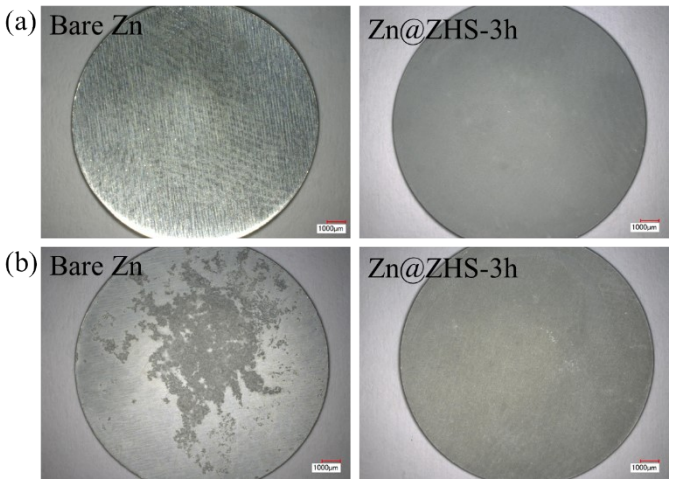

Figure S25. Photographs of bare Zn and Zn@ZHS-3h anodes in symmetric cells (a) before and (b) after 100 cycles under a current density of 1 mA cm^{-2} with a capacity of 1 mAh cm^{-2}.

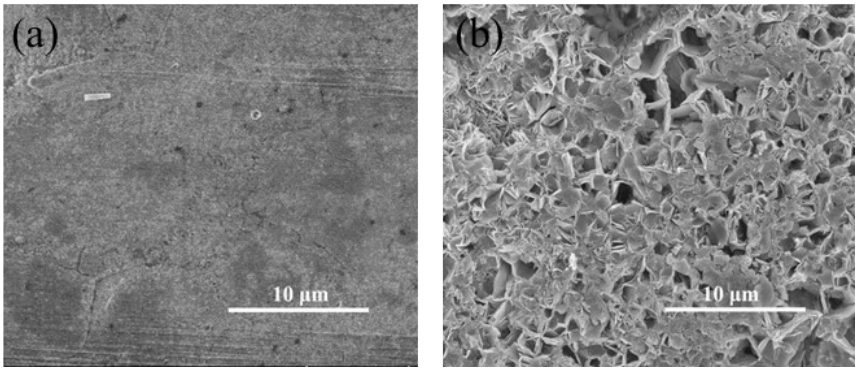

Figure S26. SEM images of (a) bare Zn and (b) Zn@ZHS-3h anodes in symmetric cells before cycles.

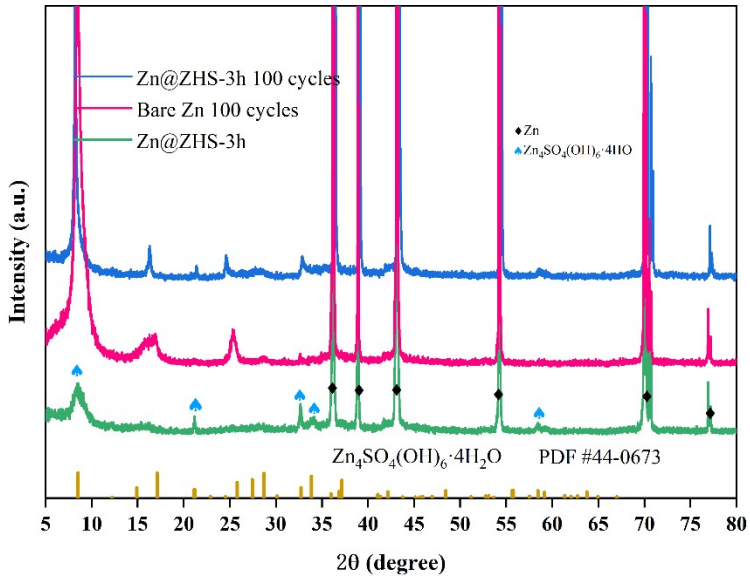

Figure S27. XRD of bare Zn and Zn@ZHS-3h anodes in symmetric cells after 100 cycles at 1 mA cm^{-2} with a capacity of 1 mAh cm^{-2}.

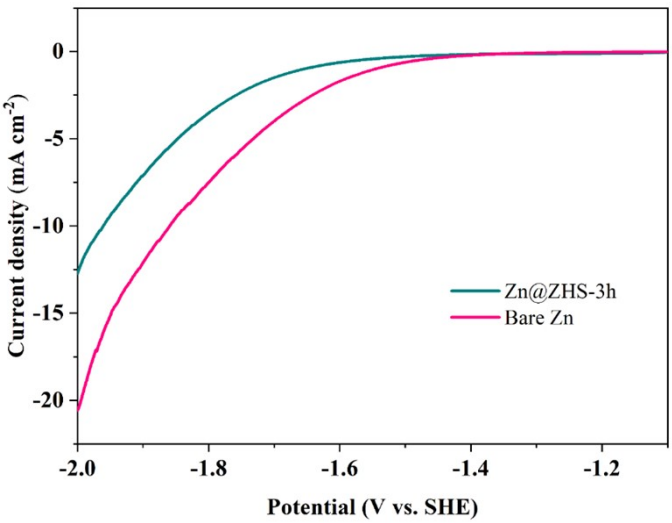

Figure S28. Linear sweep voltammetry (LSV) curves of bare Zn and Zn@ZHS-3h electrodes in 2 M Na_2SO_4 aqueous electrolyte at a scan rate of 5 mV s^{-1}.

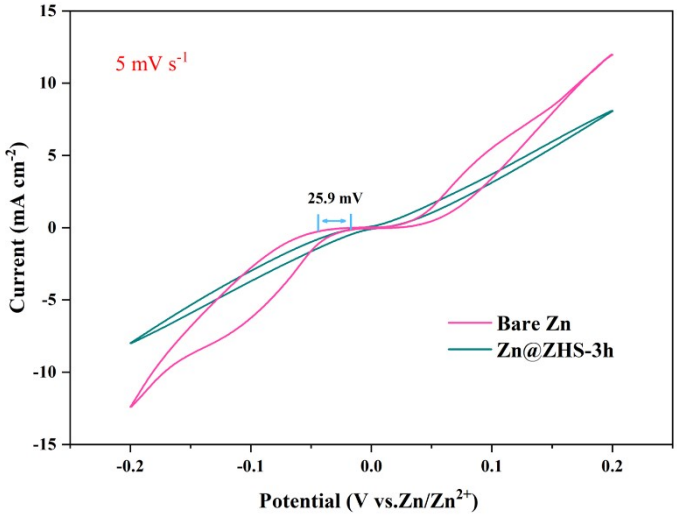

Figure S29. CV curves of bare Zn and Zn@ZHS-3h symmetric cells.

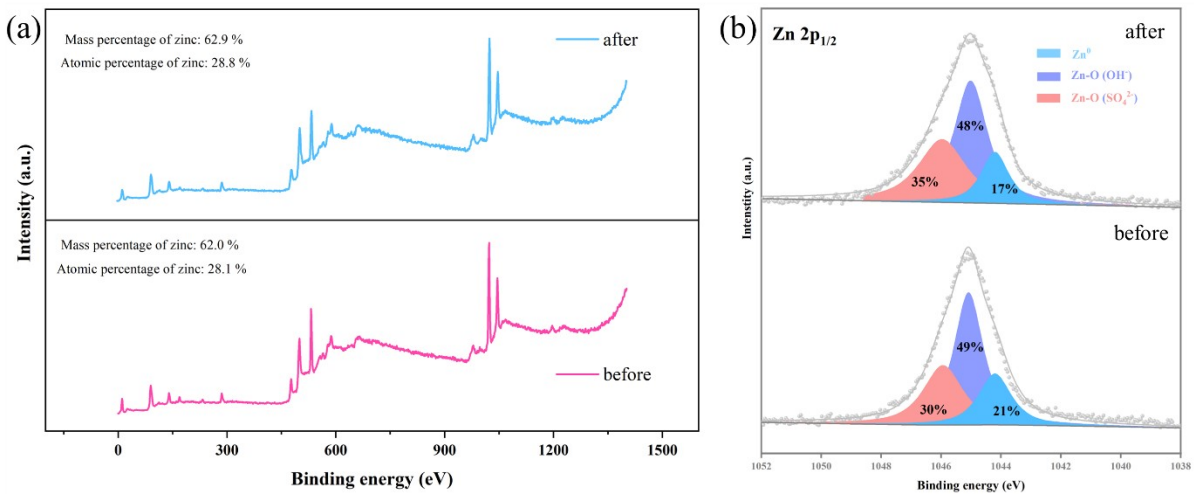

Figure S30. (a) XPS survey spectra and (b) XPS high-resolution Zn $2p_{1/2}$ spectra of Zn@ZHS-3h before and after immersing in $ZnSO_4$ solution.

A piece of Zn@ZHS-3h specimen was cut into halves. One half was immersed in $ZnSO_4$ solution and then washed thoroughly and rigorously for XPS characterization, in comparison with another half. The Zn content at the surface layer increased by 0.7 at. %, suggesting the effective adsorption of Zn^{2+} by ZHS. Meanwhile, the ratio of Zn-O (SO_4^{2-}) bond in XPS high-resolution Zn $2p_{1/2}$ spectra increased by 5%, confirming the chemical adsorption between Zn^{2+} and the electronegative O atoms of the SO_4^{2-} groups.

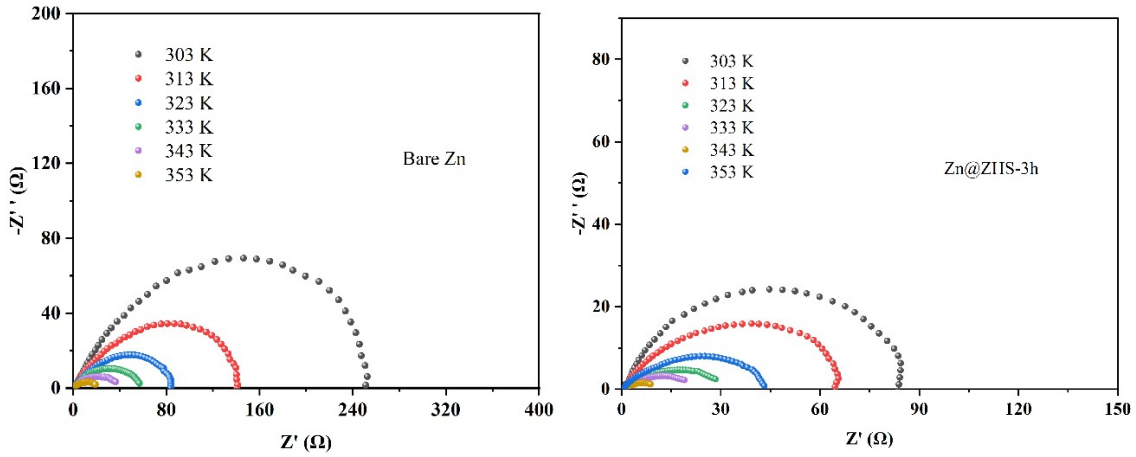

Figure S31. Nyquist plots at different temperatures for bare Zn and Zn@ZHS-3h symmetric cells.

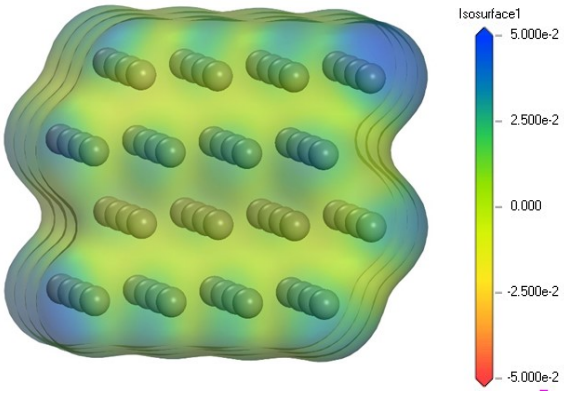

Figure S32. Electrostatic potential (ESP) distribution of bare Zn, where the positively charged part is shown in blue and the negatively charged part is shown in red.

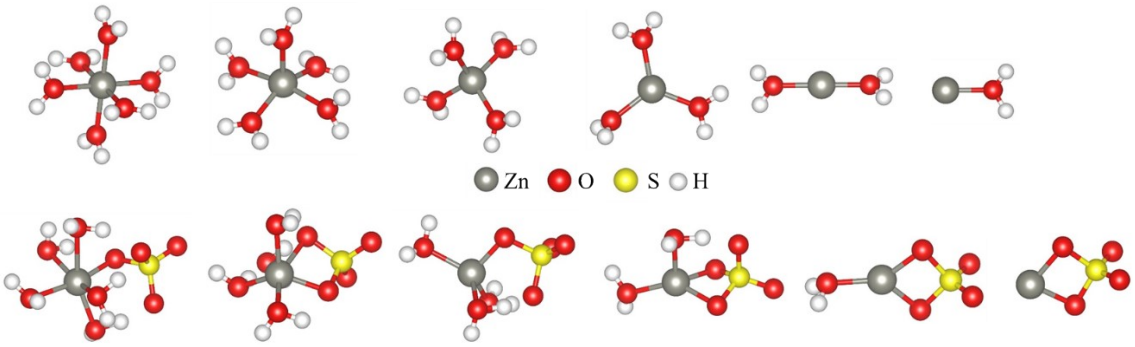

Figure S33. Molecular geometries of the $[Zn^{2+}(H_2O)_6]$ and $[Zn^{2+}(H_2O)_5(SO_4^{2-}\text{-ZHS})]$ desolvation processes.

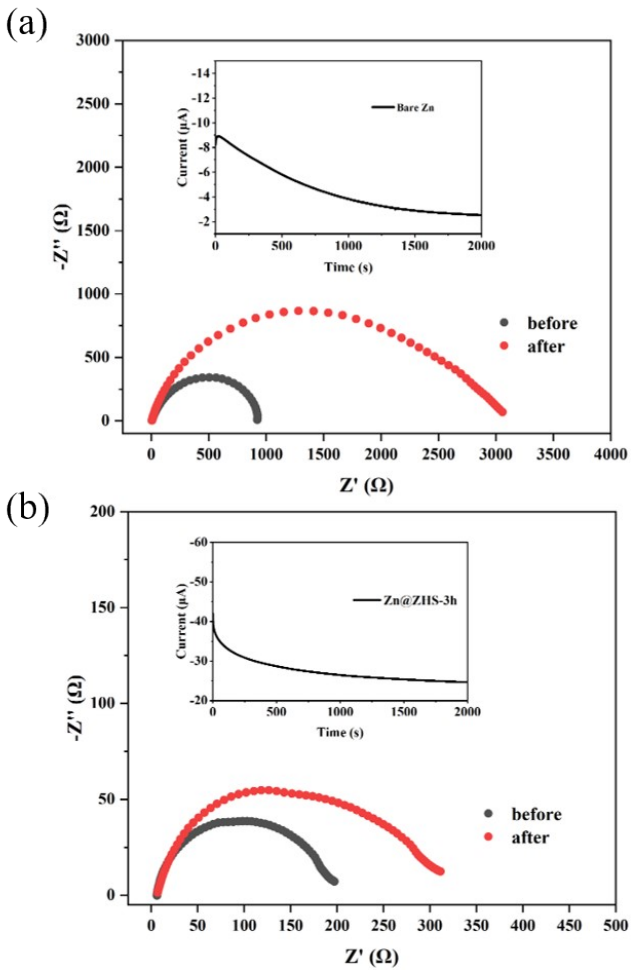

Figure S34. Polarisation profile and Nyquist plots before and after polarization of (a) bare Zn and (b) Zn@ZHS-3h symmetric cells. The Zn^{2+} transfer numbers of bare Zn and Zn@ZHS-3h can be calculated to be 0.58 and 0.41, respectively.